2024 IEEE/RSJ International Conference on Intelligent Robots and Systems (IROS)
October 14-18, 2024. Abu Dhabi, UAE

Research of calibration method for fusion of LDS sensor and ToF low-cost sensor

Jiahui Zhu[1],Guitao Yu[2], Yang He[2],Kui Yang[1] ,Dongtai Liang[1]*

***Abstract*—This paper proposes a method for calibrating the external parameters of the LDS sensor and ToF depth camera based on three cylinders. This method obtains the scanning data of the side surfaces of the three cylinders at different postures by changing the posture of the robot. For the single-line laser plane scanned by the LDS sensor, three elliptical contours are obtained by intersecting with the side surfaces of the three cylinders respectively. The Random Sample Consensus (RANSAC) algorithm is used to obtain the coordinates of the center points of the three elliptical contours and two random points on each elliptical contour. For the three-dimensional point cloud image of the cylinder scanned by the ToF depth camera, the RANSAC algorithm is used to fit the central axis of the three cylinders. The nonlinear optimization equation is established using the three center points obtained from the three elliptical contours and the distances from the two random points on each elliptical contour to their corresponding central axes. In this paper, we propose to use a fusion method of the Powell algorithm and the BFGS algorithm to solve the nonlinear optimization equations to obtain the transformation matrix between the LDS sensor and the ToF depth camera. Finally, simulation and actual test are carried out based on the proposed method, and the influence of the initial value of the calibration parameter on the calibration result is discussed. The accuracy of the calibration algorithm in this paper is verified through comparative experiments of the calibration algorithm. The results show that the calibration accuracy of the proposed method is better than that of the traditional planar calibration method, and it has the characteristics of simple operation and high calibration accuracy.**

I. INTRODUCTION

The calibration problems of LDS sensor and ToF depth cameras [1] are very important in robotics applications, and they are two fairly representative sensors in the field of Simultaneous Localization and Mapping (SLAM). Camera-based vision SLAM [2] can utilize the rich texture information in the image, but is susceptible to light interference [3]. Lidar-based laser SLAM [4] can directly acquire depth information of measurement points, but is prone to degradation and failure in scenes with missing features such as corridors, tunnels, and glass walls [5]. In this paper,ToF depth camera is used to provide a dense point cloud image of the environment and LDS sensor to provide a sparse point cloud image.LDS sensor and camera data fusion can realize the complementary information of two sensors and get richer 3D environment information, which is widely used in remote sensing measurement, autonomous driving, robotics and other fields [6].

In our case, ToF depth camera and LDS sensor are used in combination on a mobile robot for map building and navigation work. In order to effectively fuse the sensor data, it is crucial to accurately estimate the status pose between the sensors. In this paper, we present a calibration method based on constraints from the side surfaces of three cylinders. Firstly, by changing the robot's position, we obtain the scanning data of the cylindrical sides under different positions i.e., the center point of the cylinder fitted by the laser contour and the distance constraints from two random points on the laser contour to the central axis of the cylinder, then we use the data of the scanning data of the cylindrical sides to build nonlinear optimization equations, and finally, the calibration parameters are obtained by solving the equations using the fusion method of Powell algorithm and BFGS algorithm. The main contributions of this paper can be summarized as follows:

- A calibration method based on three cylinders for LDS sensors and ToF depth cameras has been proposed.
- A method combining Powell algorithm and BFGS algorithm was proposed to solve nonlinear optimization equations.
- Compared with other planar calibration methods, this paper provides more adequate constraints and only requires one observation for calibration.
- The calibration results using the three-cylinder object and combined with the algorithm in this paper are not affected by the fluctuation of the initial values of the calibration parameters within a certain range.

The rest of this paper is organized as follows: Sec.II presents the related works, Sec.III introduces our work in detail, Sec.IV shows the experiment results, and conclusions are discussed in Sec.V.

II. RELATED WORK

The robotic system in this paper relies on LDS sensors and ToF depth cameras to measure geometric features of the environment.In order to fuse the information acquired by these two sensors, the relative position between them needs to be precisely known. For 3D lidar, it is easier to establish the correspondence between the two sensors, as compared to 2D laser's single line data that provides only one line, 3D laser's multi-line data provides information about the point cloud surface [7]. External calibration of a single line lidar is more challenging because the point cloud data of a single line lidar provides information in only two dimensions,and additional constraints must be used for calibration with the camera.

We are grateful for financial support from the Ningbo Public Welfare Science and Technology Plan Project (2022S004) .
*Corresponding author.
[1]Ningbo University, Ningbo, Zhejiang, China
[2]Healthy & Intelligent Kitchen Engineering Research Center of Zhejiang Province

The calibration of lidar and camera has been previously performed mainly using a checkerboard grid, and zhang et al. [8] proposed an external parameter calibration method for camera and single-line lidar in 2004, using point-to-plane constraints. However, for the relative position between the camera and lidar from a single input observation, only two degrees of freedom are constrained. As a result, the method requires a large number of different observations to ensure the accuracy of the calibration.Vasconcelos et al. [9] addressed the shortcomings in [8] by forming a perspective three-point (P3P) problem, giving a closed-form method for solving for the external parameters in 6 degrees of freedom, where the minimum number of laser observations required becomes 3 frames (each frame of observation providing two valid constraints) due to the estimation of 6 parameters. However, this method requires high accuracy of the input data and is susceptible to noise.Naroditsky et al. [10] used point-to-line constraints in the plane to achieve calibration between two sensors without initialization, but a large number of different observations are required to obtain reasonable results.

There are many similar studies, most of the algorithms use a planar calibration plate, which loses one dimension of constraints during the calibration process and is prone to overfitting problems [11]. Dong et al. [12] used a V-shaped calibration mode composed of two non coplanar triangles, and the single observation point to surface constraint was sufficient to uniquely constrain the relative attitude between the two sensors. Therefore, the accuracy requirement for obtaining the plane was relatively high.Gomez-Ojeda et al. [13] used two different types of constraints, i.e., line-and-plane and point-and-plane constraints, which are richer constraints than the previous planar or V-plate dependent schemes.However, the calibration accuracy is highly dependent on the right angles between the three orthogonal planes, which are difficult to make precisely 90° in practice. The right angle between the two walls usually affects laser measurements when multiple observations from different angles are required to obtain additional accuracy.Hu et al. [14] further extended the work [13] by deriving a minimum solution from a single input observation. However, the solution is obtained through two processes (calibration between the trihedron and the lidar, and calibration between the trihedron and the camera), thus accumulating errors due to data noise in each process. Specifically, in the calibration between the trihedron and the camera, they determine the scale of the translation by using the actual lengths of the two edges of the trihedron, which is inconvenient to construct and difficult to measure accurately. Pusztai et al. [15] used a trihedron for calibration and established point-to-point constraints by detecting the vertices of the calibration board to obtain high-precision extrinsic parameters. However, this algorithm requires manual removal of background point clouds and manual annotation of image corners.

III. PROPOSED METHOD

A. Calibration program design

For the calibration problem of the LDS sensor and ToF depth camera mounted on the robot, this paper proposes a calibration scheme based on three cylinders. Firstly, three cylinders are placed at an arbitrary position in the robot workspace, and these three cylinders are placed side by side. The position of the robot is adjusted so that the LDS sensor and the sides of the three cylinders intersect, and the intersection shape is an ellipse. Fig. 1. shows the calibration model with point-line constraints of our method, and the transformation matrix of the LDS sensor coordinate system Σ_L with respect to the ToF depth camera coordinate system Σ_c is $\boldsymbol{T}_{CL}$, which is the calibration matrix. At different robot positions, the Elliptical center point obtained by intersecting the LDS sensor and the three cylinders laterally are $\boldsymbol{O}_j$, $\boldsymbol{O}_{j+1}$ and $\boldsymbol{O}_{j+2}$. Any two points on the three ellipse lines obtained by intersecting the lidar and the three cylinders are obtained randomly using the RANSAC algorithm for a total of six points $\boldsymbol{Q}_j$, $\boldsymbol{Q}_{j+1}$, $\boldsymbol{Q}_{j+2}$,$\boldsymbol{Q}_{j+3}$, $\boldsymbol{Q}_{j+4}$, $\boldsymbol{Q}_{j+5}$. Since the output of the LDS sensor is 2-dimensional contour data in a single line laser coordinate system, the z-value of this contour point cloud data is constant at 0. The contour data j is：

$$\boldsymbol{L}_L^j = [\boldsymbol{p}_1, \boldsymbol{p}_2, \boldsymbol{p}_3, \cdots, \boldsymbol{p}_k] = \begin{bmatrix} x_1 & x_2 & x_3 & \cdots & x_k \\ y_1 & y_2 & y_3 & \cdots & y_k \\ 0 & 0 & 0 & 0 & 0 \end{bmatrix} \tag{1}$$

$\boldsymbol{p}_i = [\, x_i, y_i, 0\,]^T$, $i = 1, 2, \cdots, k$ in the above equation is the coordinate of the point in the 2D contour point cloud.

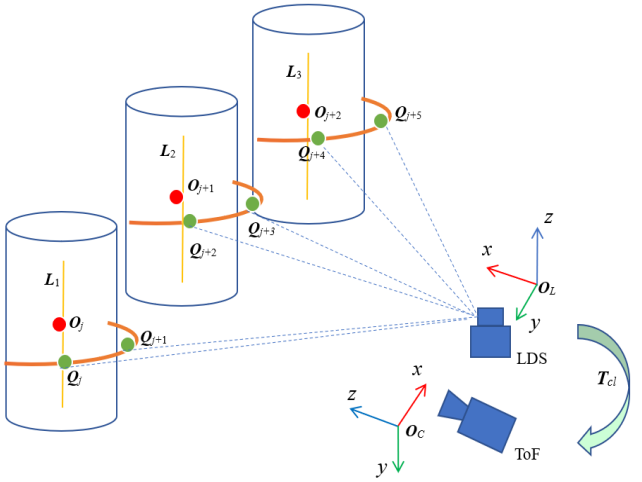

Fig. 1. Point-line constrained calibration models. The LDS sensor and ToF sensor use three side-by-side cylinders as calibration objects, so that the three lidar contour lines and the three cylindrical surfaces are aligned, and geometric constraints between the two sensors are established to estimate external parameters.

By using homogeneous transformation to transform $\boldsymbol{L}_L^j$ into the ToF depth camera coordinate system, the three-dimensional point cloud data $\boldsymbol{L}_C^j$ of the elliptical contour in the ToF depth camera coordinate system is obtained as follows:

$$\begin{bmatrix} \boldsymbol{L}_C^j \\ 1 \end{bmatrix} = \boldsymbol{T}_{CL} \begin{bmatrix} \boldsymbol{L}_L^j \\ 1 \end{bmatrix} = \boldsymbol{T}_{CL} \begin{bmatrix} p_1 & p_2 & p_3 & \cdots & p_k \\ 1 & 1 & 1 & \cdots & 1 \end{bmatrix} \tag{2}$$

$\boldsymbol{T}_{CL}$ is the calibration matrix, then the contour data $\boldsymbol{Z}$ is

$$\boldsymbol{Z} = \left[\boldsymbol{L}_C^j \right], j = 1, 2, \cdots m \tag{3}$$

Since the positions of the three cylinders are fixed, the points in the profile scan data $\boldsymbol{Z}$ of the LDS sensor are constrained to be on the same cylinder side. The equation is established based on the constraint principle that the laser profile is tangent to the sides of the three cylinders. The optimization problem of the nonlinear equation is solved by the fusion method of the Powell algorithm and the BFGS algorithm, and finally an accurate calibration matrix is obtained. The calibration scheme is shown in Fig. 2.

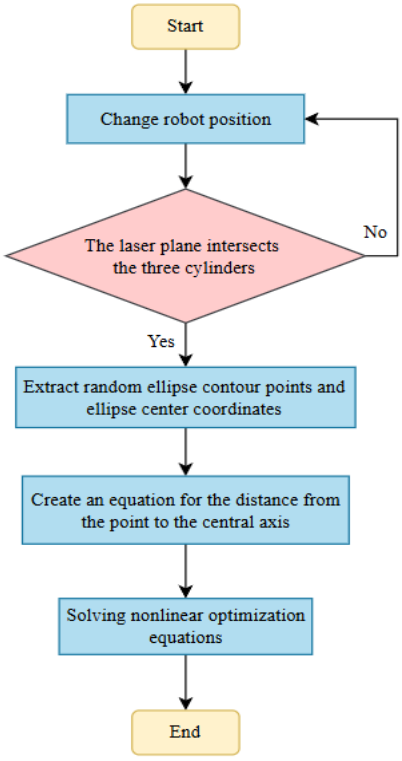

Fig. 2. Flow chart of the calibration program. In the calibration process, the distance equations from the laser point to the central axis of the cylinder in different attitudes are obtained by changing the robot's position, and the calibration matrix is obtained by solving the equation.

B. Calibration modeling

Since the shape of the intersection of the laser plane and the cylinder is elliptical, the laser contour is elliptical, the elliptical fitting of the filtered point cloud data is carried out by using the random sampling consistency algorithm to obtain the coordinates of the center points of three elliptical contours and the coordinates of two random points on each elliptical contour. Among them, the equation of the elliptical contour is:

$$\boldsymbol{A}x^2 + \boldsymbol{B}xy + \boldsymbol{C}y^2 + \boldsymbol{D}x + \boldsymbol{E}y + 1 = 0 \tag{4}$$

The equations $\boldsymbol{A}$, $\boldsymbol{B}$, $\boldsymbol{C}$, $\boldsymbol{D}$, $\boldsymbol{E}$ are the parameters of the elliptic equation.

The calibration algorithm in this paper is based on the constraint on the three cylindrical sides, that is, minimizing the distance between all laser profile data and the cylindrical sides [16]. This constraint is implemented by using the constraint equations of the following two conditions.

1) The distance from the fitted circle center points $\boldsymbol{O}_j$, $\boldsymbol{O}_{j+1}$, and $\boldsymbol{O}_{j+2}$ in the LDS sensor coordinate system to the fitted central axis in the ToF depth camera coordinate system is 0. According to the ellipse profile equation the coordinates of the ellipse center point can be obtained as:

$$\begin{cases} \boldsymbol{x}_L = \dfrac{\boldsymbol{BE} - 2\boldsymbol{CD}}{4\boldsymbol{AC} - \boldsymbol{B}^2} \\ \boldsymbol{y}_L = \dfrac{\boldsymbol{BD} - 2\boldsymbol{AE}}{4\boldsymbol{AC} - \boldsymbol{B}^2} \\ \boldsymbol{z}_L = 0 \end{cases} \tag{5}$$

According to the characteristics of coordinate homogeneous transformation, the point $\boldsymbol{O}_j(x_C, y_C, z_C)$ is obtained by transforming the ellipse center point $\boldsymbol{O}_j(x_L, y_L, 0)$ into the ToF depth camera coordinate system, that is:

$$\begin{bmatrix} x_C \\ y_C \\ z_C \\ 1 \end{bmatrix} = \boldsymbol{T}_{CL} \begin{bmatrix} x_L \\ y_L \\ 0 \\ 1 \end{bmatrix} = \begin{bmatrix} a_{11} & a_{12} & a_{13} & t_1 \\ a_{21} & a_{22} & a_{23} & t_2 \\ a_{31} & a_{32} & a_{33} & t_3 \\ 0 & 0 & 0 & 1 \end{bmatrix} \begin{bmatrix} x_L \\ y_L \\ 0 \\ 1 \end{bmatrix} \tag{6}$$

The remaining two ellipse center point conversion equations are the same. Since the elliptical center point $\boldsymbol{O}_j$ has a constant value of 0 in the Z-axis coordinates in the sensor coordinate system, from the above equation, the elements a_{13}, a_{23} and a_{33} have no effect on the solution result,the parameters we need to calibrate at this moment are [a_{11}, a_{21}, a_{31}, a_{12}, a_{22}, a_{32}, t_1, t_2, t_3].Assuming that a point $\boldsymbol{P}(x_0, y_0, z_0)$ on the cylindrical axis and the direction vector of the axis $\boldsymbol{N} = [m, l, n]$ are known in the ToF Depth Camera coordinate system, the equation of the cylindrical axis is:

$$\frac{x - x_0}{m} = \frac{y - y_0}{l} = \frac{z - z_0}{n} \tag{7}$$

Connecting the ellipse center point $\boldsymbol{O}_j(x_C, y_C, z_C)$ and a point $\boldsymbol{P}(x_0, y_0, z_0)$,on the axis to form the line segment $\boldsymbol{O}_j\boldsymbol{P}$, the length of projection $\boldsymbol{L}$ of the line segment $\boldsymbol{O}_j\boldsymbol{P}$ on the cylindrical axis is:

$$\boldsymbol{L} = \begin{bmatrix} m & l & n \end{bmatrix} \begin{bmatrix} x_C - x_0 \\ y_C - y_0 \\ z_C - z_0 \end{bmatrix} \tag{8}$$

Then the square d_j^2 of the distance from the point $\boldsymbol{O}_j$ to the axis of the cylinder is:

$$\begin{aligned} \boldsymbol{d}_j^2 &= |\boldsymbol{O}_j\boldsymbol{P}|^2 - \boldsymbol{L}^2 \\ &= [(x_C - x_0)^2 + (y_C - y_0)^2 + (z_C - z_0)^2] - \\ &\quad [m(x_C - x_0) + l(y_C - y_0) + n(z_C - z_0)]^2 = 0 \end{aligned} \tag{9}$$

2) In the LDS sensor coordinate system, there are three arcs in one observation, and two points are randomly extracted on each arc. Therefore, six laser points can be extracted in one observation, namely $\boldsymbol{Q}_j$, $\boldsymbol{Q}_{j+1}$, $\boldsymbol{Q}_{j+2}$, $\boldsymbol{Q}_{j+3}$, $\boldsymbol{Q}_{j+4}$, and $\boldsymbol{Q}_{j+5}$.The theoretical distance of each of the six laser points to the fitted

median axis in the ToF depth camera coordinate system is the radius of the column R. Similarly, the The square d_i^2 of the distance from one of the points to the cylindrical axis is the square of the cylindrical radius R^2.

$$\begin{aligned} d_i^2 &= |\boldsymbol{Q}_j\boldsymbol{P}|^2 - \boldsymbol{L}^2 \\ &= [(x_C - x_0)^2 + (y_C - y_0)^2 + (z_C - z_0)^2] - \\ &[m(x_C - x_0) + l(y_C - y_0) + n(z_C - z_0)]^2 = R^2 \end{aligned} \tag{10}$$

By changing the robot's position and posture, we can obtain multiple sets of laser contour data. We use the RANSAC algorithm to fit the center point of each laser contour, and randomly extract two points on each elliptical contour to find the distance from the center point of each elliptical contour and the two points on the contour to the cylinder axis. Under ideal conditions, the center point $\boldsymbol{O}_j$ lies on the axis of the cylinder, i.e., $d_j^2 = 0$, where $j = 1, 2, ..., k$. The distance from the two points on the side of the cylinder to the axis of the cylinder for each elliptical contour is the radius of the cylinder, R, i.e., $d_j^2 = R^2$, where $i = 1, 2, ..., k$. The calibration problem is transformed into an optimization problem for solving nonlinear equations. It is known that the parameters to be calibrated for the required solution are $[a_{11}, a_{21}, a_{31}, a_{12}, a_{22}, a_{32}, t_1, t_2, t_3]$, and that:

$$\begin{cases} \boldsymbol{f}_n(\boldsymbol{x}) = d_j^2 \\ \boldsymbol{g}_n(\boldsymbol{x}) = d_i^2 - R^2 \\ \boldsymbol{F}(\boldsymbol{x}) = [\boldsymbol{f}_n(\boldsymbol{x}), \boldsymbol{g}_n(\boldsymbol{x})], n = 1, 2, \ldots, k \end{cases} \tag{11}$$

$F(x)$ is a function with multiple unknowns. We hope to find a set of solutions that minimize the following equation and thus obtain the calibration parameters:

$$\min \boldsymbol{F}(\boldsymbol{x}) \tag{12}$$

The lidar-to-camera translation matrix $\boldsymbol{t} = [t_1, t_2, t_3]$, and the first two columns of the rotation matrix $\boldsymbol{R}_{cl}$, $\boldsymbol{r}_1 = [a_{11}, a_{21}, a_{31}]^T$, and $\boldsymbol{r}_2 = [a_{12}, a_{22}, a_{32}]^T$. Once we have solved for the first two columns of $\boldsymbol{R}_{cl}$,$\boldsymbol{r}_1$ and $\boldsymbol{r}_2$, the third column $\boldsymbol{r}_3$ can be found by the following equation:

$$\boldsymbol{r}_3 = \boldsymbol{r}_1 \times \boldsymbol{r}_2 \tag{13}$$

However, the rotation matrix obtained using the above approach does not satisfy the properties of a rotation matrix $\boldsymbol{R}^T\boldsymbol{R} = \boldsymbol{I}_{3\times3}$ (where $\boldsymbol{I}$ is a 3 × 3 unit matrix). Assuming that the desired rotation matrix is $\hat{\boldsymbol{R}}_{cl}$, it can be estimated by computing the minimized Frobenius norm problem with constraints:

$$\text{argmin} \,\| \hat{\boldsymbol{R}}_{cl} - \boldsymbol{R}_{cl} \|_F, \text{subject to } \hat{\boldsymbol{R}}_{cl}^{\,T} \hat{\boldsymbol{R}}_{cl} = \boldsymbol{I} \tag{14}$$

In layman's terms, the meaning of the above equation is to find a matrix $\hat{\boldsymbol{R}}_{cl}$ that is closest to $\boldsymbol{R}_{cl}$ and satisfies the rotation matrix property $\boldsymbol{R}^T\boldsymbol{R} = \boldsymbol{I}_{3\times3}$ as an outer parameter.

C. Solving the calibration model

For the problem of solving nonlinear optimization equations, Powell's algorithm can be used, in which the first n search directions in each iteration must be kept linearly independent, otherwise the optimal solution of the problem will never be obtained, which is the main drawback of Powell's algorithm. The method of fusion of Powell algorithm and BFGS algorithm, however, can accelerate the convergence speed through fine parameter optimization on the basis of global search in order to find the optimal solution as soon as possible. This avoids the defect that the original Powell algorithm is easy to degrade during iteration.

1) Powell's algorithm: Powell's algorithm is a conjugate direction method, since it only needs to calculate the objective function value without having to find the derivative value. Therefore Powell's algorithm is more practical than the ordinary conjugate direction method (conjugate gradient method), using Powell's algorithm to solve has the advantages of high accuracy, fast convergence and strong local search ability [17]. Iterative steps of Powell's algorithm:

STEP 1: Given the initial point $\boldsymbol{X}_0$, the number of iteration rounds $k = 1$, $\boldsymbol{X}_0^{(k)} = \boldsymbol{X}_0$, dimension n, and convergence accuracy ε;

STEP 2: Enter the direction of the coordinate axis as the search direction for the first round:

$$\boldsymbol{S}_i^{(k)} = \boldsymbol{e}_i, \boldsymbol{e}_i = \left[0, \cdots 1, 0, \cdots, 0\right]^T (i = 1, 2, \cdots, n) \tag{15}$$

STEP 3: Starting from $\boldsymbol{X}_0^{(k)}$, we perform n one-dimensional searches along the direction $\boldsymbol{S}_i^{(k)}$ in turn, and obtain n one-dimensional minima $\boldsymbol{X}_i^{(k)}$($\boldsymbol{i}$ = 1, 2,⋯, $\boldsymbol{n}$). The connection points are $\boldsymbol{X}_0^{(k)}$ and $\boldsymbol{X}_n^{(k)}$, and the first conjugate direction is constructed:

$$\boldsymbol{S}_{n+1}^{(k)} = \boldsymbol{X}_n^{(k)} - \boldsymbol{X}_0^{(k)} \tag{16}$$

STEP 4:A one-dimensional search along $\boldsymbol{S}_{n+1}^{(k)}$ from $\boldsymbol{X}_n^{(k)}$ yields the minima point $\boldsymbol{X}_{n+1}^{(k)}$ (completing one round of iterations);

STEP 5: Here are the convergence accuracy judgments, if $\| \boldsymbol{X}_{n+1}^{(k)} - \boldsymbol{X}_0^{(k)} \| \leqslant \varepsilon$ is satisfied, output $\boldsymbol{X}^* = \boldsymbol{X}_{n+1}^{(k)}$ and end. Otherwise, eliminate $\boldsymbol{S}_i^{(k)}$ and add $\boldsymbol{S}_{n+i}^{(k)}$, which constitutes the search direction for the k+1st round:

$$\boldsymbol{S}_i^{(k+1)} = \boldsymbol{S}_{i+1}^{(k)} \ (i = 1, 2, \cdots, n) \tag{17}$$

STEP 6: Put $\boldsymbol{X}_{n+1}^{(k)} \rightarrow \boldsymbol{X}_0^{(k+1)}$, make $k = k+1$ and return to step 3.

2) Fusion of Powell algorithm and BFGS algorithm: Powell basic algorithm has a strong reference value in theory. It is a search method formed by the property of conjugate direction to accelerate the convergence speed. However, for multi-dimensional complex functions, it is easy to fail to solve the minimum value using only Powell algorithm. Because in the Powell basic algorithm, there is no measurement of whether the n search directions will become linearly related. Once the search directions are related, conjugate directions cannot be formed, resulting in degeneration and dimensionality reduction. In order to avoid the above problems, this paper proposes a method to fuse the Powell algorithm and the BFGS algorithm. By fusing with the two algorithms, the success rate of solving the optimization equation can be improved. The specific process is as follows:

STEP 1: Initialization parameters: set the initial parameter vector $\boldsymbol{x}_0$, the iteration counter k, the maximum number of iterations and the convergence threshold ε.

STEP 2: Initialize the Hessian matrix $\boldsymbol{B}_0$ of the BFGS approximation as a unit matrix.

STEP 3: Enter the loop until the termination conditions are satisfied (For example, the maximum number of iterations is reached or the residuals are less than the threshold):

a. Calculate the gradient $\boldsymbol{g}_k$ of the current parameter vector $\boldsymbol{x}_k$.

b. Update the Hessian matrix $\boldsymbol{B}_k$ using BFGS,Calculate search direction:

$$\boldsymbol{d}_k = -\boldsymbol{B}_k \boldsymbol{g}_k \tag{18}$$

c. Determine the step size α_k using the line search method; Set the initial step size $\alpha = 1$;Select a suitable line search method; Find the optimal step size α_k that satisfies the line search condition by gradually decreasing the step size in each iteration.

d. Update parameter vector:

$$\boldsymbol{x}_{(k+1)} = \boldsymbol{x}_k + \alpha_k \boldsymbol{d}_k \tag{19}$$

e. Compute the gradient $\boldsymbol{g}_{(k+1)}$ of the new parameter vector $\boldsymbol{x}_{(k+1)}$.

f. Update the Hessian matrix $\boldsymbol{B}_{(k+1)}$ of the BFGS approximation with the Powell direction.

Compute the Powell direction:

$$\boldsymbol{p}_k = \boldsymbol{x}_{(k+1)} - \boldsymbol{x}_k \tag{20}$$

Compute the Powell update formula:

$$\begin{cases} \boldsymbol{y} = \boldsymbol{g}_{(k+1)} - \boldsymbol{g}_k \\ \boldsymbol{s} = \alpha_k \boldsymbol{d}_k \\ \boldsymbol{B}_{(k+1)} = \boldsymbol{B}_k - \dfrac{\boldsymbol{B}_k \boldsymbol{s}\, \boldsymbol{s}^T \boldsymbol{B}_k}{\boldsymbol{s}^T \boldsymbol{B}_k \boldsymbol{s}} + \dfrac{\boldsymbol{y}\, \boldsymbol{y}^T}{\boldsymbol{y}^T \boldsymbol{s}} \end{cases} \tag{21}$$

g. Updating the Iteration Counter:

$$k = k + 1 \tag{22}$$

STEP 4: Return the optimal solution $\boldsymbol{x}^*$.

In the above process, the BFGS algorithm is used to approximate the update of the Hessian matrix, while the Powell direction is used to guide the search direction. The Powell-BFGS fusion algorithm can gradually optimize parameters and find the optimal solution during the iteration process by calculating gradients, updating the Hessian matrix, calculating the Powell direction, and determining the step size of each iteration. This fusion algorithm can overcome the local optimal problem in traditional gradient descent algorithms, improve the accuracy and convergence speed of optimization.

IV. EXPERIMENTS

The ToF depth camera selected in this paper is Sunny Optical's Cleaner01F1 (linear ToF depth camera module), with an accuracy of ±1.5cm; the LDS sensor selected is Ledong's STL-06P single-line laser lidar, with an accuracy of ±1cm. The effectiveness of the algorithm in this paper is verified by simulation comparison experiments with the algorithm in [8], and the influence of the initial value of the calibration parameters on the calibration results is analyzed.

A. Simulation Comparison Experiment

The calibration data are first obtained by scanning the three cylinders with a LDS sensor and ToF depth camera, and then the results are analyzed based on the calibration data, i.e., the trend of the accuracy of the rotation and translation matrices obtained by the calibration algorithm according to the different number of iterations. According to the work of Geiger et al. [18], the accuracy of the externally calibration can be evaluated by the linear translation error and the angular error:

$$\boldsymbol{e}_t = \left\| \boldsymbol{t} - \boldsymbol{t}_{gt} \right\|_2 \tag{23}$$

$$\boldsymbol{e}_r = arc\cos\left(\frac{tr(\boldsymbol{R}^{-1}\boldsymbol{R}_{gt}) - 1}{2} \right) \tag{24}$$

Where $\boldsymbol{R}_{gt}$ and $\boldsymbol{t}_{gt}$ are the truth values of the rotation and translation matrices, respectively, and $tr(\cdot)$ is the trace of the matrix.

Due to the inability to accurately obtain the transformation matrix between ToF depth cameras and LDS sensors in the real world, this paper conducts comparative testing of the algorithm on the GAZEBO simulation platform, and verifies the effectiveness of the proposed method based on simulated measurement data.The simulation platform is equipped with ToF depth camera and LDS sensor, the translation between the camera and lidar is set to t_x = 0.15m,t_y = 0m, t_z = 0.02m.The rotation is set to θ_{roll} = 1.57 rad, θ_{pitch} = 1.57 rad, θ_{yaw} = 0 rad.

In order to verify the accuracy of the camera and Lidar external parameter calibration, 10 sets of simulation data are collected for testing, and each set of data contains 20 observations. Table I counts the simulation test results of this paper's method and the original Powell algorithm.

In the simulation experiments, the average translation error and the average angular error of this paper's method are smaller than that of the original Powell algorithm, which indicates that the calibration method of this paper has better estimation accuracy of the translation matrix and the rotation matrix than that of the original Powell algorithm.

TABLE I SIMULATION TEST RESULTS

	$\boldsymbol{e}_t$ (cm)			$\boldsymbol{e}_r$ (rad)		
	max	min	mean	max	min	mean
Our method	0.58	0.22	0.32	0.22	0.09	0.15
Origin Powell	0.92	0.42	0.68	0.75	0.25	0.56

B. Effect of initial values of calibration parameters on calibration results

In order to verify the influence of the initial value of the calibration parameters on the calibration results, the random errors of the ToF depth camera and the LDS sensor are not considered. Change the robot's position, record the scanning data of the camera and lidar under different robot postures, set

the initial value of the calibration parameters taken as different calibration parameters according to the value characteristics of different parameters in the calibration parameters, respectively, substituting into this paper's algorithm, the original Powell's algorithm, and the algorithm of the paper [8] to solve the optimization equations for the minimum value, and repeat the 10 groups of comparative experiments to record the value of the solution of each group, and the results are shown in Table II.

TABLE II
EFFECT OF INITIAL VALUES OF CALIBRATION PARAMETERS ON CALIBRATION RESULTS

Number	Our method	Origin Powell	Zhang [8]
1	5.686025×10^{-8}	7.450147×10^{-8}	1.193164×10^{-7}
2	6.923522×10^{-7}	FAILURE	FAILURE
3	8.931273×10^{-8}	9.540358×10^{-8}	$2.440300e\times10^{-7}$
4	7.869194×10^{-7}	2.460388×10^{-7}	1.774233×10^{-7}
5	8.637951×10^{-7}	8.540978×10^{-8}	2.246818×10^{-8}
6	5.867464×10^{-7}	FAILURE	FAILURE
7	5.980337×10^{-8}	8.630362×10^{-7}	FAILURE
8	8.00225×10^{-7}	FAILURE	5.904808×10^{-8}
9	2.310467×10^{-7}	5.620032×10^{-7}	5.240658×10^{-7}
10	4.250354×10^{-7}	7.210624×10^{-7}	FAILURE
Success	**100%**	**70%**	**60%**

In a given optimization problem, the algorithm is considered to have converged when the maximum number of paradigms of the gradient is less than or equal to a set threshold. Where the solution result is less than 10^{-6} represents a successful calibration, and greater than 10^{-6} can be judged as a failure of the algorithm's calibration. As can be seen from Table II, the initial value of the calibration parameter has a great influence on the paper [8] algorithm to solve the optimization equations, in 10 groups of experiments, 4 groups of solution results can not converge, only 6 groups of solution results converge, and its calibration success rate is 60%. For the original Powell algorithm, its calibration success rate is 70%. The calibration success rate of our algorithm is 100%, which shows that this algorithm is not affected by the initial value of the calibration parameters.

C. *Comparative experiments on calibration algorithms*

In order to investigate the effect of different calibration algorithms on the calibration results, calibration simulation experiments are performed based on the algorithm in this paper, the original Powell algorithm, and the algorithm in paper [8].

For the algorithm in paper [8], as shown in Fig. 3, it is different from the previous point-to-line constraints. Firstly, the RANSAC algorithm is used to fit the central axis of the three cylinders and the coordinate origin of the camera to form the plane $\boldsymbol{T}_j$, $\boldsymbol{T}_{j+1}$, $\boldsymbol{T}_{j+2}$ respectively, and then a fourth plane $\boldsymbol{T}_{j+3}$ is fitted according to the central axis of the three cylinders, and a point on the central axis of the three cylinders is taken as $\boldsymbol{P}_j$, $\boldsymbol{P}_{j+1}$, $\boldsymbol{P}_{j+2}$ respectively, such that $\boldsymbol{P}_j$, $\boldsymbol{P}_{j+1}$, $\boldsymbol{P}_{j+2}$ are in the plane $\boldsymbol{T}_j$, $\boldsymbol{T}_{j+1}$, $\boldsymbol{T}_{j+2}$ respectively, and also satisfy that $\boldsymbol{P}_j$, $\boldsymbol{P}_{j+1}$, $\boldsymbol{P}_{j+2}$ are on the plane $\boldsymbol{T}_{j+3}$. In one frame of observation LDS sensor and camera scanning three cylinders get a total of six constraints.

Suppose the plane is parameterized by $\boldsymbol{\pi}^c = [\boldsymbol{n}^c, d] \in \boldsymbol{R}^4$ in the camera coordinate system Σ_c, where $\boldsymbol{n}^c \in \boldsymbol{R}^3$ is the three-dimensional normal vector of the plane and d is the distance from the origin of the camera coordinate system to the plane. A three-dimensional point on the plane has coordinates $\boldsymbol{P}^c \in \boldsymbol{R}^3$ in the camera coordinate system, and the point on the plane satisfies:

$$\boldsymbol{n}^{cT}\boldsymbol{p}^c + \boldsymbol{d} = 0 \tag{25}$$

The rotation and translation matrices between the laser coordinate system Σ_L to the camera coordinate system Σ_c is $\boldsymbol{R}_{cl}$ and $\boldsymbol{t}_{cl}$. If it is known that a laser point $\boldsymbol{p}^l$ on the cylindrical axis in the laser coordinate system falls in the plane, the constraint that the point is in the plane enables the equations to be constructed with respect to the outer parameters:

$$\boldsymbol{n}^{cT}(\boldsymbol{R}_{cl}\boldsymbol{P}^l + \boldsymbol{t}_{cl}) + d^c = 0 \tag{26}$$

The above equation is able to provide a constraint, and six constraints can be obtained through one frame of scanning by the method in Fig. 3. The initial value is first obtained through several frames of constraints, and then the initial value is then optimized using multiple sets of scans to obtain more accurate calibration results.

The calibration accuracies of the algorithm of paper [8], the original Powell algorithm, and the algorithm of this paper are compared in Fig. 4, where 10 sets of scanning data at different robot positions are acquired using the LDS sensor and the camera, with each set containing 30 observations, and a subset of 5, 10, 15, and 20 observations are randomly selected from each set of 30 observations to perform the calibration. The first and second plots indicate the mean values of the estimated rotation and translation errors of the three algorithms as the number of observations of the three cylinders by the LDS sensor and the camera increases.

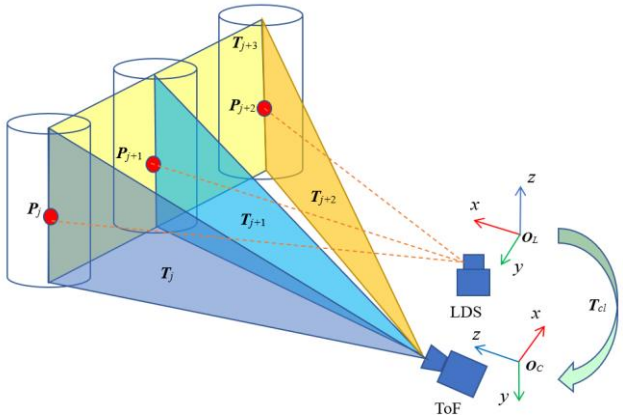

Fig. 3. Point-plane constrained calibration models. The model mainly consists of the constraints that the center points of the ellipses lie on the corresponding planes.

The third and fourth plots indicate the standard deviation of the estimated rotation and translation errors of the three algorithms as the number of observations increases. As can be seen from the results in Fig. 4, the average errors over 20 observations are 0.37° and 3.2 mm, which are much lower than those of the original Powell algorithm (0.8° and 8.2 mm) and the algorithm of paper [8] (1.2° and 13mm). In addition, our algorithm yields reasonable calibrations with only 5 observations.

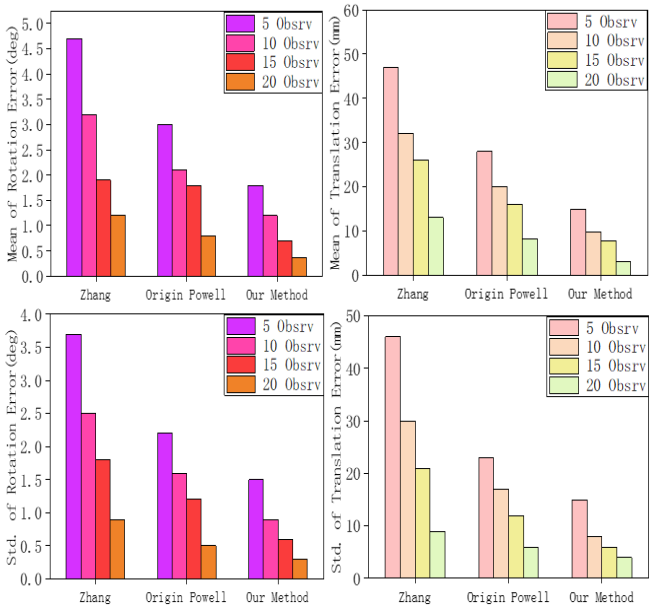

Fig. 4. Observation error.Containing the mean of the rotation and translation errors for the three algorithms, and the standard deviation.

D.Real Scene Validation

The two algorithms were calibrated on a robot equipped with a ToF depth camera and an LDS sensor. The experimental platform is shown in Fig. 5.

In order to verify the accuracy of the calibration results of the algorithm in this paper compared with the algorithm in the paper [8], a calibration experimental platform based on three cylinders was built. By changing the robot's posture multiple times, the ToF depth camera can completely scan the three cylinders, and the lidar plane intersects with the sides of the three cylinders.

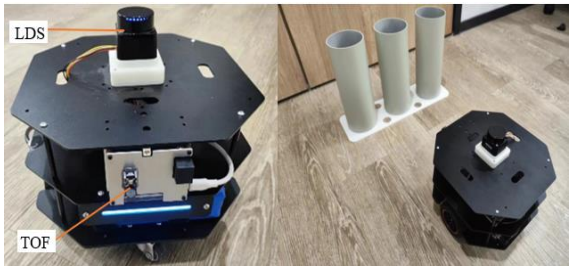

Fig. 5. Calibration of the experimental platform.ToF depth camera and LDS sensor mounted on a mobile robot.

Using the algorithm of this paper and the algorithm of paper [8], 20 observations are completed, and the respective transformation matrices are obtained, and the distance from the center of each ellipse to the axis of the columns is calculated from the obtained transformation matrices. The smaller the distance from the center of the ellipse to the cylinder axis, the higher the calibration accuracy. According to the obtained transformation matrices, as shown in Fig. 6, 20 sets of scanning data from the ToF depth camera and the LDS sensors are recorded respectively, and each set of observations contains three laser ellipse center points. From the statistical results in Table III, it can be seen that, through 60 measurements, the maximum value of the distance *d* from the center point of the laser fitting circle to the central axis of the cylinder in the algorithm of this paper is 8.9 mm, the minimum value is 2.9 mm, and the average value is 6.2 mm. The maximum value of the distance *d* from the center point of the laser fitting circle to the central axis of the cylinder in the algorithm of the paper [8] is 13.7 mm, the minimum value is 4.8 mm, and the average value is 8.4 mm. This result verifies that the calibration algorithm in this paper is more accurate than the algorithm in paper [8].

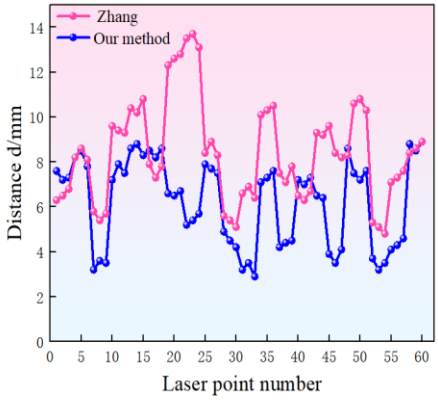

Fig. 6. Distance from point to line.Distance from the center point of the ellipse contour to the axis of the cylinder.

TABLE III RESULTS OF DISTANCE STATISTICS

	max(mm)	min(mm)	mean(mm)
Our Method	8.9	2.9	6.2
Zhang [8]	13.7	4.8	8.4

In order to verify the effectiveness of the proposed method in the actual scene, the algorithm proposed in this paper is compared with the algorithm proposed in the paper [8]. First, the two methods input 20 sets of observations respectively to obtain the calibration results, and then use the 3D visualization platform rviz in ROS to observe the results of the two methods calibrating the TOF depth camera and LDS sensor, as shown in Fig. 7. The method proposed in this paper obtains the white laser outline, and the method proposed in the paper [8] obtains the red laser outline. The green point cloud is the 3D point cloud cylindrical image generated by the ToF depth camera.

As can be seen from Fig. 7, the point cloud of the white LDS sensor has a higher degree of overlap with the point cloud of the ToF depth camera, and the method proposed in this paper can obtain a more reasonable calibration result. Therefore, this experiment verifies the accuracy of the calibration method proposed in this paper.

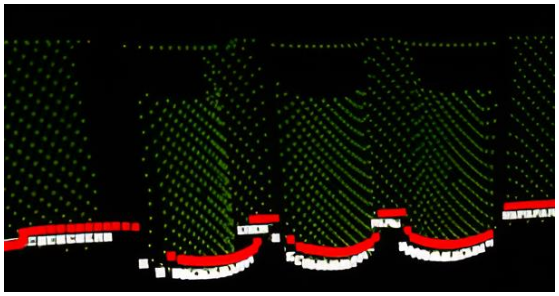

Fig. 7. Calibration results. The green point cloud is the point cloud image of the three cylinders scanned by the ToF depth camera, the red point cloud is the point cloud scanned by the method in the paper [8], and the white point cloud is the point cloud scanned by the method in this paper.

V. CONCLUSION

For the calibration problem of LDS sensor and ToF depth camera, a calibration method using three cylinder side constraints is proposed. This method requires three standard cylinders placed side by side. The calibration process is simple and easy to operate. Simulation experimental results show that the point-to-line constraint based on the cylinder side is better and more accurate than the point-to-surface constraint in the algorithm of paper [8].

Using the constraints of the three standard cylinder sides, the calibration problem is transformed into an optimization problem for solving nonlinear equations. This paper uses a fusion method of the Powell algorithm and the BFGS algorithm to solve the equations, which has a faster convergence speed and stronger robustness, improving the accuracy and success rate of calibration.

In practical applications, the calibration algorithm between sensors needs to be characterized by convenience, accuracy and speed. Although the algorithm in this paper has good convenience and accuracy, the method of solving nonlinear optimization equations using the fusion of Powell's algorithm and BFGS algorithm also increases the computational complexity of the algorithm, which involves switching and balancing between two different algorithms in order to obtain the best performance and convergence. Therefore, an in-depth study of the algorithms for solving nonlinear optimization equations and balancing the stability between the two algorithms is the focus of the subsequent studies.

REFERENCES

[1] Z. Li, H. Dong, D. Liu and Y. Ding, "Extrinsic Calibration of a 2D Laser Rangefinder and a Depth-camera Using an Orthogonal Trihedron," *2022 IEEE/RSJ International Conference on Intelligent Robots and Systems (IROS)*, Kyoto, Japan, 2022, pp. 6264-6269.

[2] R. Mur-Artal, J. M. M. Montiel and J. D. Tardós, "ORB-SLAM: A Versatile and Accurate Monocular SLAM System," in *IEEE Transactions on Robotics*, vol. 31, no. 5, pp. 1147-1163, Oct. 2015.

[3] J. Engel, V. Koltun and D. Cremers, "Direct Sparse Odometry," in *IEEE Transactions on Pattern Analysis and Machine Intelligence*, vol. 40, no. 3, pp. 611-625, 1 March 2018.

[4] J. Zhang and S. Singh. "LOAM: Lidar odometry and mapping in real-time." *Robotics: Science and systems*. vol. 2, No. 9, pp. 1-9, July. 2014.

[5] Shi, J. H., Wang, Q., & Feng, Y. Y. "Camera calibration method based on 3D calibration plate." *Transducer and Microsystem Technologies*, vlo.40, no. 6, pp. 48-51, 2021.

[6] Shiqiang, W., Zhaozong, M., Nan, G., & Zonghua, Z. "Advancements in fusion calibration technology of lidar and camera. " *Infrared and Laser Engineering*, vol. 52,no. 8,pp. 1-14, April. 2023.

[7] L. Zhou, Z. Li and M. Kaess, "Automatic Extrinsic Calibration of a Camera and a 3D LiDAR Using Line and Plane Correspondences," *2018 IEEE/RSJ International Conference on Intelligent Robots and Systems (IROS)*, Madrid, Spain, 2018, pp. 5562-556.

[8] Qilong Zhang and R. Pless, "Extrinsic calibration of a camera and laser range finder (improves camera calibration)," *2004 IEEE/RSJ International Conference on Intelligent Robots and Systems (IROS) (IEEE Cat. No.04CH37566)*, Sendai, Japan, 2004, pp. 2301-2306 vol.3.

[9] F. Vasconcelos, J. P. Barreto and U. Nunes, "A Minimal Solution for the Extrinsic Calibration of a Camera and a Laser-Rangefinder," in *IEEE Transactions on Pattern Analysis and Machine Intelligence*, vol. 34, no. 11, pp. 2097-2107, Nov. 2012.

[10] O. Naroditsky, A. Patterson and K. Daniilidis, "Automatic alignment of a camera with a line scan LIDAR system," *2011 IEEE International Conference on Robotics and Automation*, Shanghai, China, 2011, pp. 3429-3434.

[11] D. Tsai, S. Worrall, M. Shan, A. Lohr and E. Nebot, "Optimising the selection of samples for robust lidar camera calibration," *2021 IEEE International Intelligent Transportation Systems Conference (ITSC)*, Indianapolis, IN, USA, 2021, pp. 2631-2638.

[12] W. Dong and V. Isler, "A Novel Method for the Extrinsic Calibration of a 2D Laser Rangefinder and a Camera," in *IEEE Sensors Journal*, vol. 18, no. 10, pp. 4200-4211, 15 May15, 2018.

[13] R. Gomez-Ojeda, J. Briales, E. Fernandez-Moral and J. Gonzalez-Jimenez, "Extrinsic calibration of a 2d laser-rangefinder and a camera based on scene corners," *2015 IEEE International Conference on Robotics and Automation (ICRA)*, Seattle, WA, USA, 2015, pp. 3611-3616.

[14] Z. Hu, Y. Li, N. Li and B. Zhao, "Extrinsic Calibration of 2-D Laser Rangefinder and Camera From Single Shot Based on Minimal Solution," in *IEEE Transactions on Instrumentation and Measurement*, vol. 65, no. 4, pp. 915-929, April 2016.

[15] Pusztai, Z., Eichhardt, I., & Hajder, L. Accurate calibration of multi-lidar-multi-camera systems. *Sensors*, vol. 18, no. 7, pp. 21-39, 2018.

[16] Gao, J., Liang, D., & Chen, Y. A Hand-eye Calibration Method of Line Laser Profile Scanning Robot Based on Standard Cylinder. *J iqiren/Robot*, vol. 44, no. 3, pp. 321-332, 2022.

[17] Xia Guimei,Su Changhui. Simplified particle swarm algorithm based on Powell search method[J]. *Journal of Ningxia University(Natural Science Edition),*vol. 36 no. 02, pp. 126-130, 2015.

[18] A. Geiger, F. Moosmann, Ö. Car and B. Schuster, "Automatic camera and range sensor calibration using a single shot," *2012 IEEE International Conference on Robotics and Automation*, Saint Paul, MN, USA, 2012, pp. 3936-3943.